

Magnetic Localization Algorithm of Capsule Robot Based on BP Neural Network

Qiang Fu^{ID}, Dongdong Zhao^{ID}, Lei Shao^{ID}, and Songyuan Zhang^{ID}, Member, IEEE

Abstract—To explore the positioning tracking problem of capsule endoscopy, the advantages of magnetic positioning technology as a solution are highlighted. Considering that the capsule robot is small and cannot have enough built-in driving and positioning tracking devices, new technical means are needed to solve this problem. Therefore, we propose a prediction method based on the BP neural network model to locate the position of the robot in the magnetic field. To evaluate the accuracy of a BP neural network model with three hidden layers, the predicted results of the model, the results of the nonlinear algorithm, and the actual coordinate points were compared to determine whether it could accurately predict the actual coordinate points. We set the criterion for correct localization as the Euclidean distance between the predicted coordinate point and the actual coordinate point being less than 0.01 mm, and obtained the localization rates of the nonlinear localization algorithm and the neural network prediction method as 46.7% and 95.2%, respectively. By comparing the results, it is found that the positioning accuracy predicted by the BP neural network is higher and has higher accuracy. This shows that the prediction accuracy of the algorithm is more optimized, which can meet the real-time and positioning accuracy requirements of the capsule endoscope.

Index Terms—BP neural network, capsule robot, magnetic dipole model, magnetic positioning, nonlinear positioning algorithm.

I. INTRODUCTION

AS PEOPLE'S lifestyles change, they are increasingly seeking medical services that are comfortable and efficient. Traditionally, cable endoscopes were used as the primary method for diagnosing and treating gastrointestinal diseases. However, this method could cause patients discomfort and scratch their gastrointestinal tract during insertion. To address these issues, researchers both domestically and internationally

Manuscript received 19 August 2023; revised 16 November 2023; accepted 17 November 2023. Date of publication 8 January 2024; date of current version 11 January 2024. This work was supported in part by the Innovative Cooperation Project of Tianjin Scientific and Technological Support under Grant 18PTZWHZ00090 and in part by the Graduate Education Reform Fund of Tianjin University of Technology under Grant YBXM2203. The Associate Editor coordinating the review process was Dr. Huang-Chen Lee. (*Corresponding authors:* Lei Shao; Songyuan Zhang.)

Qiang Fu and Lei Shao are with the Tianjin Key Laboratory of New Energy Power Conversion, Transmission and Intelligent Control, the School of Electrical Engineering and Automation, Tianjin University of Technology, Tianjin 300380, China (e-mail: fuqiang@email.tjut.edu.cn; Shaolei555@163.com).

Dongdong Zhao is with the School of Electrical Engineering and Automation, Tianjin University of Technology, Tianjin 300384, China (e-mail: 2904784297@qq.com).

Songyuan Zhang is with the State Key Laboratory of Robotics and Systems, Harbin Institute of Technology, Harbin 150001, China (e-mail: zhangsy@hit.edu.cn).

Digital Object Identifier 10.1109/TIM.2023.3341129

have been focusing on developing capsule endoscopy in recent years.

However, one of the challenges faced by medical capsule robots is their limited positioning space, which makes it difficult to achieve precise positioning during medical inspections. To overcome this challenge, scholars have conducted extensive research on the localization system of capsule robots. Among them, the method based on the magnetic Jacobian matrix is a commonly used technique. Slawinski et al. [1] proposed an algorithm for eliminating uncertainty errors using the sensitivity ellipsoid model of the magnetic Jacobian matrix. The algorithm adjusts the pose estimate based on the difference between sensor measurements and a preset value and uses a sensitivity ellipsoid model to estimate the margin of error. This approach can improve localization accuracy and robustness. Natali et al. [2], [3], and Son et al. [4] also respectively proposed an iterative method based on the Jacobian matrix to solve the real-time positioning problem of the magnetically controlled capsule robot. They proposed a synchronous calibration method for the magnetic positioning and drive system [2], [3], [4]. Hu et al. [5] reduced the error of the objective function by calibrating the position, direction, sensitivity, and other parameters of the magnetic sensor. In addition, methods based on magnetic sensor arrays are also a popular technique. Hu et al. [6] designed a tracking system for the spatial position and orientation of permanent magnets, while Pham and Aziz [7] developed a real-time localization system using an array of magnetic sensors. Shao and Guo [8] optimized the signal-to-noise ratio of magnetic sensors and selected the optimal positioning algorithm and sensor ratio to reduce the pose error. Song et al. [9] introduced a multitarget positioning and recognition method based on a magnetic sensor array. Popek et al. [10] proposed a noniterative method for positioning and driving a magnetic capsule endoscope using a rotating magnetic dipole field, which can calculate the six-degree-of-freedom (6-DOF) position and attitude of the capsule endoscope based on data from an external magnetic field sensor. In addition, there are some methods based on image localization. You et al. [11] proposed a six-dimensional hybrid localization algorithm that combines image localization and magnetic sensor position. To this end, we also intend to improve the localization method of capsule robots during their movement inside the human body, to enhance their localization accuracy and stability. However, during this movement, the capsule robot can be affected by various interference factors, such as changes in the magnetic field, peristalsis of the gastrointestinal tract, and rotation of the capsule robot. These

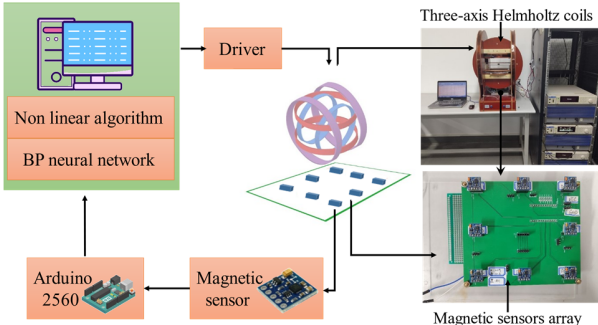


Fig. 1. Process of the wireless microrobotic robot control system and the corresponding practical experimental platform.

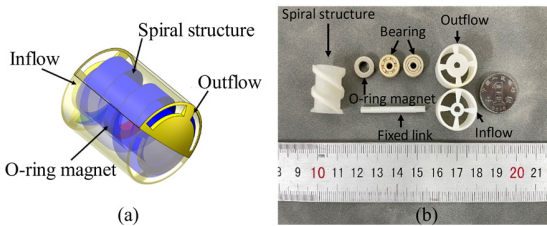


Fig. 2. (a) Model of the spiral jet microrobot. (b) Structure of microrobot.

factors could cause errors and instability in the measured values of the magnetic sensor. Therefore, we propose a location prediction method based on the BP neural network algorithm, which can improve prediction accuracy by training a large amount of data and can be applied to many different location problems. The BP neural network training and learning method proposed by us can adaptively adjust the weight and threshold of the positioning algorithm according to different internal environments of the human body, to achieve accurate positioning in various complex environments.

In this article, we propose a localization prediction algorithm method based on the BP neural network, which can realize real-time prediction of capsule robots. Through the analysis of experimental data, the validity and reliability of the algorithm are verified, and it is proved that the BP neural network algorithm has higher accuracy in predicting and positioning.

II. EXPERIMENTAL PLATFORM

A conceptual diagram of the whole for contactless data transmission using a magnetic sensor array is shown in Fig. 1. The control system comprises a three-phase power supply (KIKUSUI PCR1000LE2), three-axis Helmholtz coils, magnetic sensors array (HMC5883L), Arduino 2560, PC, and capsule robot. The capsule robot is a magnetically controlled modular robot. It has a spiral structure, a fluid shell, and an O-ring magnet as shown in Fig. 2. The capsule robot can move in fluid by generating propulsion from the rotation of its internal magnet under an external magnetic field [12]. It sends data to a PC through its magnetic sensor array, and the PC uses nonlinear algorithms and BP neural networks to calculate and predict the robot's position and orientation based on the sensor data. Finally, based on the predicted position information from the algorithms, the operator can manually adjust the current

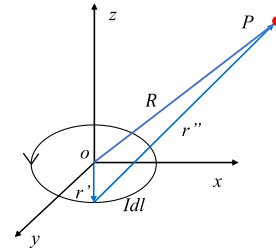


Fig. 3. Magnetic field model generated by the current loop at a point in space.

and frequency of the three-phase power supply to readjust the direction and speed of the robot, achieving closed-loop control of the entire positioning process.

III. MAGNETIC POSITIONING MATHEMATICAL MODEL

With advancements in science and technology, permanent magnet materials have become more prevalent in daily life, greatly facilitating production and enhancing convenience [13], [14]. As one of the important driving methods of capsule robots, magnetic drive technology can effectively reduce the internal space of micro-robots, reduce the weight of the fuselage, and provide hardware development conditions for the functional design of medical capsule robots. The magnetic dipole model simplifies. The permanent magnet is into a magnetic dipole and approximates the magnetic field of the permanent magnet by describing the magnetic dipole.

A. Magnetic Dipole Model

When the radius of the permanent magnet inside the capsule robot is much larger than its length, the permanent magnet can be regarded as a magnetic dipole, as illustrated in Fig. 3. In this case, the magnetic potential A can be utilized to derive the magnetic induction B . The magnetic flux density field B is the rotational of the magnetic vector potential as expressed by (1). Therefore, by calculating the gradient of the magnetic potential, the absolute position vector R , and the relative position vector r' describe the position and direction of the permanent magnet in space, and changes in these parameters will also affect the magnetic field distribution generated by the permanent magnet. This simplified model is often used when designing and analyzing microrobots such as capsule robots, as it simplifies calculations while still providing sufficient accuracy [15], [16].

$$\mathbf{B}_P = \nabla \times \mathbf{A}. \quad (1)$$

The vacuum permeability μ_0 is a constant [17], while the absolute position vector R and relative position vector r' describe the position and direction of the permanent magnet in space, and changes in these parameters will also affect the magnetic field distribution generated by the permanent magnet. Therefore, calculating the magnetic potential A by (2) can predict and control the magnetic field distribution of the permanent magnet more accurately

$$\mathbf{A}(\mathbf{r}') = \frac{\mu_0}{4\pi} \int_v \frac{\mathbf{i}(\mathbf{r}')}{r} dv. \quad (2)$$

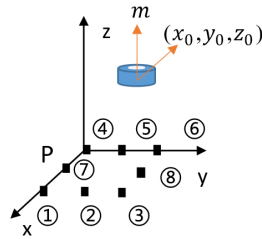


Fig. 4. Magnetic dipole model.

After simplifying (2), we get the following equation:

$$\mathbf{A}(\mathbf{r}') = \frac{\mu_0 I}{4\pi} \oint \frac{\mathbf{r} \cdot \mathbf{r}'}{r^3} d\mathbf{r}' \quad (3)$$

where I is the current intensity.

The r is defined as the distance from the measurement point to the center of mass of the permanent magnet inside the capsule robot, and \mathbf{r}' is the radius of the current loop

$$r = |\mathbf{r}' - \mathbf{r}''|. \quad (4)$$

By substituting (4) into (3) and performing Taylor expansion on (3), (5) can be obtained, which is an approximate analytical formula used to describe the distribution of the magnetic field generated by the permanent magnet

$$\mathbf{A}(\mathbf{r}') = \frac{\mu_0 I}{8\pi r'^3} \left(\oint \mathbf{r}' \times d\mathbf{r}' \right) \times \mathbf{r}. \quad (5)$$

For the convenience of calculation, we define the area S and the magnetic moment \mathbf{m} of the magnetic dipole, respectively, as follows:

$$\begin{aligned} \mathbf{m} &= IS \\ S &= \frac{1}{2} \oint \mathbf{r}'' \times d\mathbf{r}''. \end{aligned} \quad (6)$$

Through the previous derivation, the magnetic potential distribution of the magnetic field generated by the permanent magnet at any point is obtained, namely (5). Simultaneously, after bringing (6) into (5), simplifying it, and substituting it into (1), the magnetic induction intensity at point P can be obtained as follows:

$$\mathbf{B}_P = \frac{\mu_0}{4\pi} \left(\frac{3\mathbf{r}(\mathbf{m} \cdot \mathbf{r})}{r^5} - \frac{\mathbf{m}}{r^3} \right). \quad (7)$$

As shown in Fig. 4, the direction vector of the magnetic dipole moment can be expressed as $\mathbf{m} = (m_x, m_y, m_z)$.

B. Nonlinear Positioning Algorithm Model

To calculate the distribution of the magnetic field generated by the permanent magnet, it is necessary to calculate the magnitude and direction of the magnetic field, so in (8), we perform a cross-product point product operation on the magnetic induction intensity \mathbf{B} [18] at point P, the absolute potential vector \mathbf{r} and the magnetic moment \mathbf{m}

$$\mathbf{B}_P \times \mathbf{r} \cdot \mathbf{m} = 0. \quad (8)$$

By defining multiple L points in space and placing magnetic sensors array to calculate the magnetic induction intensity \mathbf{B}_p

of the corresponding points, according to the magnetic dipole model shown in (7), the magnetic source is at any point p in space (x, y, z) . The magnetic induction intensity generated can be expressed as follows:

$$\mathbf{B}_P = (B_{Px}, B_{Py}, B_{Pz}). \quad (9)$$

The vector of the geometric center of the magnetic source pointing to the space point $P(x, y, z)$ can be expressed as follows:

$$\mathbf{r} = (x - x_0, y - y_0, z - z_0). \quad (10)$$

Simplify (8) and convert it from a linear problem [18] to a nonlinear problem for solving

$$\begin{aligned} -B_{Lz}^{(i)}(y - y_0)m_x - B_{Py}^{(i)}(x - x_0)m_z - B_{Px}^{(i)}(z - z_0)m_y \\ + B_{Px}^{(i)}(y - y_0)m_z + B_{Py}^{(i)}(z - z_0)m_x + B_{Pz}^{(i)}(x - x_0)m_y = 0. \end{aligned} \quad (11)$$

We substitute (B_{Px}, B_{Py}, B_{Pz}) and the position information (x, y, z) data of the measured target point into (11) to obtain the objective function formula, the magnetic source position information (x_0, y_0, z_0) and the posture state of the capsule robot are obtained.

An inverse problem refers to the problem of finding the inputs or parameters of a system given its outputs. Due to the ill-conditioned nature of inverse problems, where small changes in the outputs can result in significant variations in the inputs or parameters, solving inverse problems requires the use of specialized mathematical methods and techniques. In this article, we transform the inverse problem into a nonlinear optimization problem. The input data is the magnetic induction intensity data measured by sensors number 1–6. Since the constraint condition of the objective function is $m_x^2 + m_y^2 + m_z^2 = 1$, it can be transformed into an optimization problem under the constraint condition. The optimization process can be summarized as follows:

$$\begin{aligned} &\min f(x) \\ &\text{s.t.} \begin{cases} A \cdot x \leq b \\ Aeq \cdot x = beq \\ c(x) \leq 0 \\ ceq(x) = 0 \\ lb \leq x \leq ub. \end{cases} \end{aligned} \quad (12)$$

A and Aeq are the constraints of the inequality and the coefficient matrix of the constraints, b and beq are the constraint vectors, and lb and ub are the upper and lower boundaries of the variables. During the solution process, we need to set an optimization option object to control certain parameters of the optimization function. The constraint tolerance in the optimization option object is set to 1e-12. This parameter is used to control the accuracy with which the optimization function meets the constraints. The step size tolerance is set to 1e-15, and the maximum number of iterations is 2000. These two parameters serve as conditions for the optimization function to stop iterating. According to these settings, the fmincon function [19] automatically searches for the optimal solution and returns the value of the optimal solution. By solving

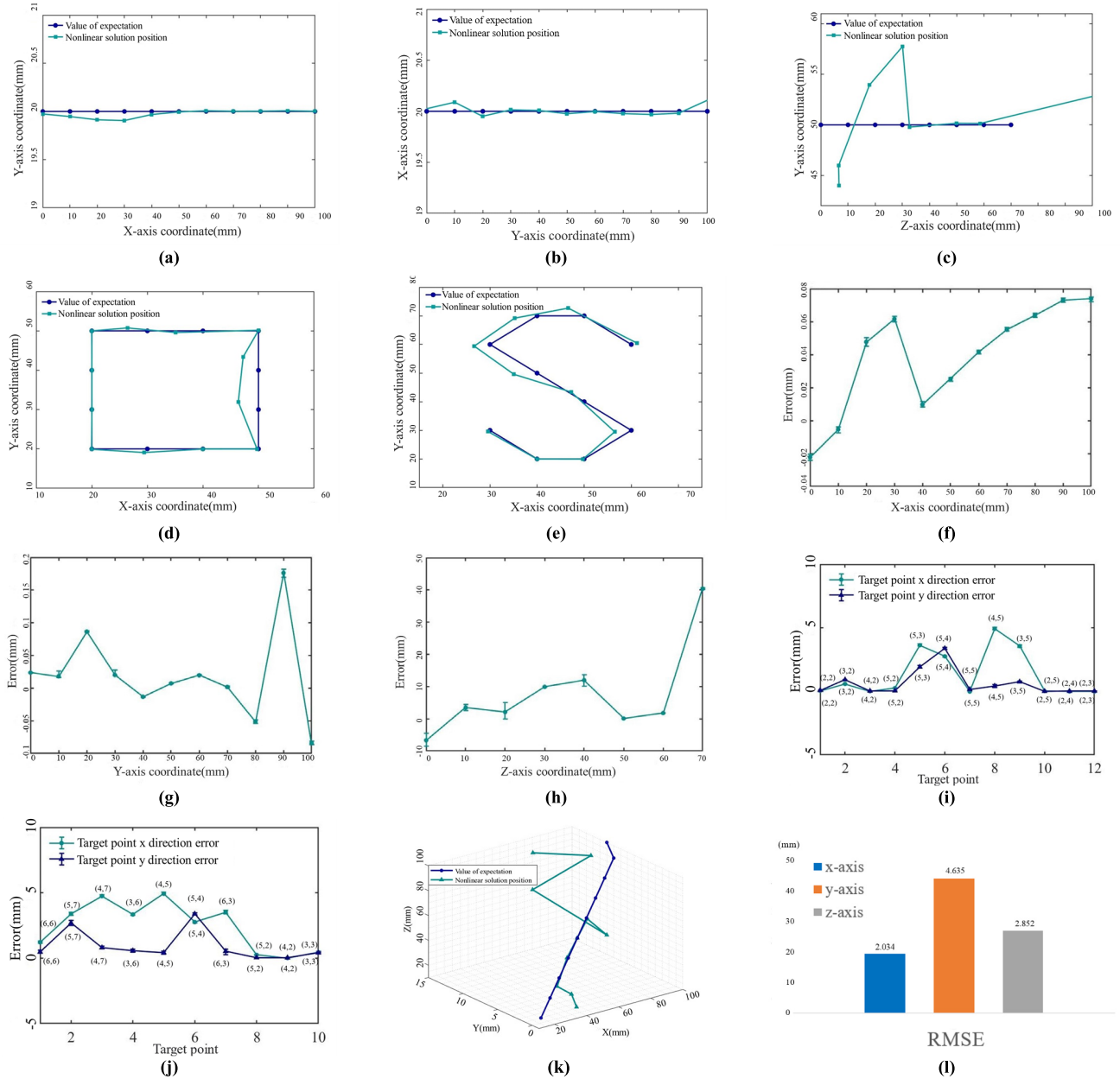


Fig. 5. Nonlinear positioning experiments. (a) x -axis direction. (b) y -axis direction. (c) z -axis direction. (d) Square path. (e) S -shaped path. (f) X -error. (g) Y -error. (h) Z -error. (i) Square-error. (j) S -error. (k) Space experiment. (l) Space experiment error.

this nonlinear programming problem in this way, the optimal solution of the magnetic source position information (x_0 , y_0 , z_0) can be calculated.

C. Nonlinear Algorithm Positioning Experiment

To analyze the error, we carried out physical experiments with different axes, different shapes, and 3-D space, respectively. We took ten sets of experiments for each item and calculated 5 times for each set.

The physical experiment result path is shown in Fig. 5, in experiments with different axes and different shapes, positioning experiments in the three directions of xyz , and square and S -shaped paths were carried out, and their errors were analyzed, and the error results are shown in Fig. 5(f)–(j). In the experiment with different axes, the y coordinate is fixed at two

first, and the positioning experiment of the permanent magnet in the x -direction is carried out, as shown in Fig. 5(a). Panel (f) is the corresponding error bar graph, which reflects the error range of the experimental data. Afterward, a positioning experiment in the y direction was carried out. In this experiment, the x coordinate of the path of the permanent magnet was fixed, and then, the y coordinate was positioned. Fig. 5(b) shows the result of the experimental path, and Fig. 5(g) is the corresponding error bar graph. In the z -axis direction, we fix the x - and y -coordinate of the permanent magnet to 5 and then position the z -coordinate. In this experiment, a sensor array is positioned within a three-axis Helmholtz coil. The sensor array is designated as the “first layer” in the physical experiment when it is located 1 cm away from the capsule robot along the z -axis. Similarly, it is designated as the “second layer”

when positioned 2 cm away from the capsule robot, and so on. A total of ten layers are established in the physical distance experiment. Since only the nonlinear calculation effect of the fifth layer is the best, and the calculation result of the R values in each data changes abruptly, the error is large, so we only keep part of the line graph of the seventh coordinate point in Fig. 5(c) to better understand Display the changing trend of the positioning path. At the same time, Fig. 5(h) is the corresponding error bar graph, which reflects the error range of the experimental data, and the error of about 4 cm may need further analysis and research to improve the accuracy and reliability of the experiment. In experiments with different shapes, positioning experiments with square and S-shaped paths were carried out. For a square path, first position at (2,2), then move 3 units in the positive x -direction, 3 units in the negative y direction, then 3 units in the negative x -direction, and finally 3 units in the negative y direction, completing the square path. As shown in Fig. 5(d), the expected path is a square, but the actual positioning result is slightly deviated, as shown in Fig. 5(i). Similarly, localization experiments for S-shaped paths were also carried out, as shown in Fig. 5(e). In this experiment, the permanent magnet moves along an S-shaped path, and the expected result is an S-shaped curve, but the actual result still has a certain deviation, as shown in Fig. 5(j).

In the 3-D experiment, we recorded the physical experiment result path of the permanent magnet from layer 1 to 10 along the z -axis and the RMSE in the three directions of the xyz -axis with a step size of 1 cm, as shown in Fig. 5(k) and (l).

IV. BP NEURAL NETWORK PREDICTION

The traditional magnetic sensors array positioning technique involves installing a magnetic source within a moving object to determine the object's spatial orientation. In space, the magnetic source generates a magnetic field within a specific range. Correspondingly, there exists a mapping relationship between the magnetic field intensity at various points in this field and the orientation of the magnetic source. Therefore, by measuring the magnetic field strength provoked by the magnetic source at a known orientation, it becomes feasible to calculate the corresponding changes in the source's orientation. Since the human body and air have similar magnetic permeability, the interference of the human body on the magnetic field of the magnetic source can be ignored.

A. BP Neural Network Prediction Model

A neuron is designed to simulate the structure of a biological neuron [20]. The basic unit of artificial neural networks is artificial neurons. The specific structure is shown in Fig. 6.

Then, the input-output relationship of the neuron is as follows:

$$y = f\left(\sum_{i=1}^n w_i x_i - \theta\right) \quad (13)$$

where $f(\cdot)$ is the activation function, y is the output of the neuron, x_i is the input of the neuron, there are n input ports in total to receive output signals from other neurons; w_i is the

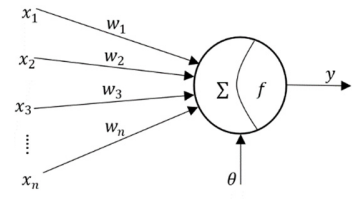


Fig. 6. Artificial neuron model.

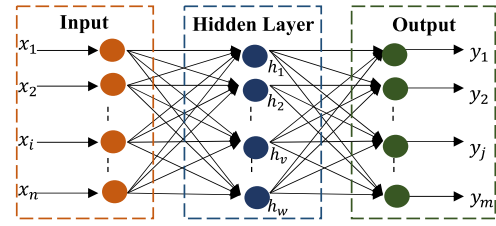


Fig. 7. BP neural network structure.

weight of the i th input of the neuron, and its size represents the degree of reception of the signal, and the positive and negative represent the impulse and inhibition of the signal. θ is the threshold of the neuron, which is most usually called "bias," and its size represents the degree of excitement of the neuron to the integrated input signal.

The back propagation neural network [21], [22] is a neural network that propagates data forward and transmits errors backward. It consists of an input layer, a hidden layer, and an output layer to form a nonlinear mapping relationship between input and output data. The basic idea is to input training sample data for feature extraction and to preprocess, then perform BP neural network training, and output the final expected result. It uses the error between the network's output response to the learning signal and the expectation as a mentor signal to adjust the network connection strength [23]. Through repeated adjustments, the error is minimized. Thus, completing the learning process. Its network model is shown in Fig. 7.

In the BP neural network, we need to define the initial parameters, let the original input vector be $X = (x_1, x_2, \dots, x_n)^T$, the output vector $H = (h_1, h_2, \dots, h_m)^T$ of the hidden layer, the output vector $O = (o_1, o_2, \dots, o_l)^T$ of the output layer, expected output vector $d = (d_1, d_2, \dots, d_l)^T$, the weight matrix $V_{ij} = (v_1, v_2, \dots, v_m)^T$, the weight matrix $W_{ij} = (w_1, w_2, \dots, w_l)^T$ between the hidden layer and the output layer and between the input layer and the hidden layer.

For the output layer and the hidden layer, there are the following expressions, where $k = 1, 2, \dots, l$, $j = 1, 2, \dots, m$

$$O_k = f(\text{net}_k), \quad \text{net}_k = \sum_{j=0}^m W_{kj} h_j \quad (14)$$

$$h_j = f(\text{net}_j), \quad \text{net}_j = \sum_{i=0}^n v_{ij} x_i. \quad (15)$$

The error between the real value and the predicted value is represented by E

$$E = \frac{1}{2} \sum_{k=1}^l (d_k - o_k)^2. \quad (16)$$

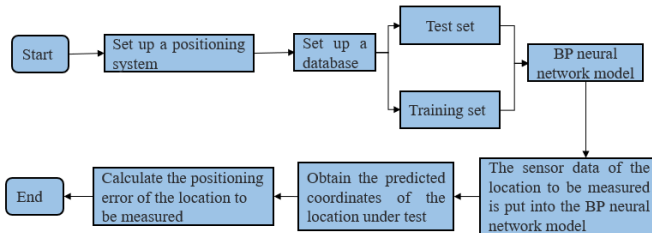


Fig. 8. Flowchart of positioning system based on BP neural network.

Bring O_k , net_k , h_j , net_j into formula (16) to have

$$E = \frac{1}{2} \sum_{k=1}^l \left\{ d_k - f \left[\sum_{j=0}^m w_{kj} f \left(\sum_{i=0}^n v_{ji} x_i \right) \right] \right\}^2. \quad (17)$$

The main purpose of the BP neural network is to repeatedly modify the weights and thresholds to minimize the value of the error function [24], [25]. In the process of error backpropagation, the weights need to be updated, where η represents the learning efficiency

$$\begin{aligned} \Delta w_{kj} &= \eta(d_k - o_k)o_k(1 - o_k)h_j \\ \Delta v_{ji} &= \eta \left[\sum_{k=1}^l \eta(d_k - o_k)o_k(1 - o_k)w_{jk} \right] h_i(1 - h_i)x_i. \end{aligned} \quad (18)$$

The number of neurons in the hidden layer can be obtained from (19), where n is the number of neurons in the input layer, m is the number of neurons (nodes) in the output layer, and a is an adjustment constant between 1 and 10

$$h_0 = \sqrt{m + n} + a. \quad (19)$$

Due to the sigmoid activation function, in line with reality, when the input value is small [26], the output value is close to 0; when the input value is large, the output value is close to 1. Therefore, the Sigmoid function is selected as the activation function of the BP neural network as follows:

$$f'(x) = \frac{e^{-x}}{(1 + e^{-x})^2} = f(x)[1 - f(x)]. \quad (20)$$

B. Comparison of the Number of Single-Target Hidden Layers

The positioning system used in this research is based on BP neural network and the specific structure is shown in Fig. 8.

To study the performance of the BP neural network in predicting magnetic induction data, we selected 100 target points in the space of $10 \times 10 \times 10$ (cm^3), each target point has 300 magnetic induction data measured by eight sensors as a training set, and another 30 data as a test set. In the experiment, the input layer of the network has eight neurons, corresponding to the xyz -axis magnetic induction intensity measured by eight sensors; the output layer has three neurons, respectively, corresponding to the xyz coordinates of the target point. By learning the data in the training set, the network can predict the corresponding output according to different inputs, indicating that the network has generalization ability and adaptability. We designed a neural network model with

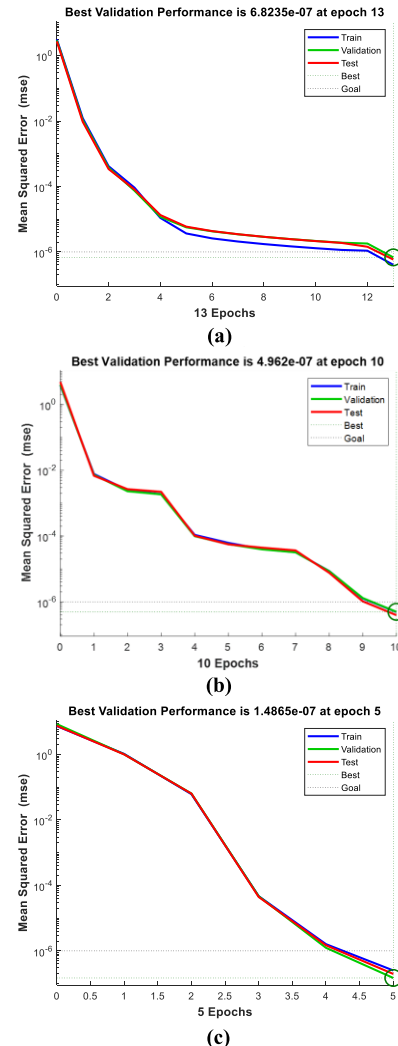


Fig. 9. MSE. (a) One layer, (b) two layers, and (c) three layers.

one to three hidden layers, and the number of neurons in the first, second, and third hidden layers was 8, 15, and 9, respectively. To better evaluate the performance of the model, we randomly select a target point (3, 2, 5) as a representative case for analysis. We conducted a network performance test of 1 to 3 hidden layers for this target point, and the test results are presented in the form of mean square error (MSE) values. Fig. 9 shows the test performance of the network with different numbers of hidden layers. It can be seen that as the number of hidden layers increases, the network achieves the best verification performance in the 13th, tenth, and fifth rounds, which are 6.8235e-07, 4.962e-07, and 1.4865e-07, respectively, indicating that the prediction accuracy of the network has been significantly improved. At the same time, it can be found that in the case of three hidden layers, the MSE value of the network drops to the minimum, which shows that the neural network model shows the best performance in the task of predicting the target point. Fig. 10 shows the fitting graph of the correlation coefficient under different numbers of hidden layers. The correlation coefficient R represents the degree of linear correlation between the predicted value and the real value, and its value is between -1 and 1 . When the R value is closer to 1 , it means that the correlation between

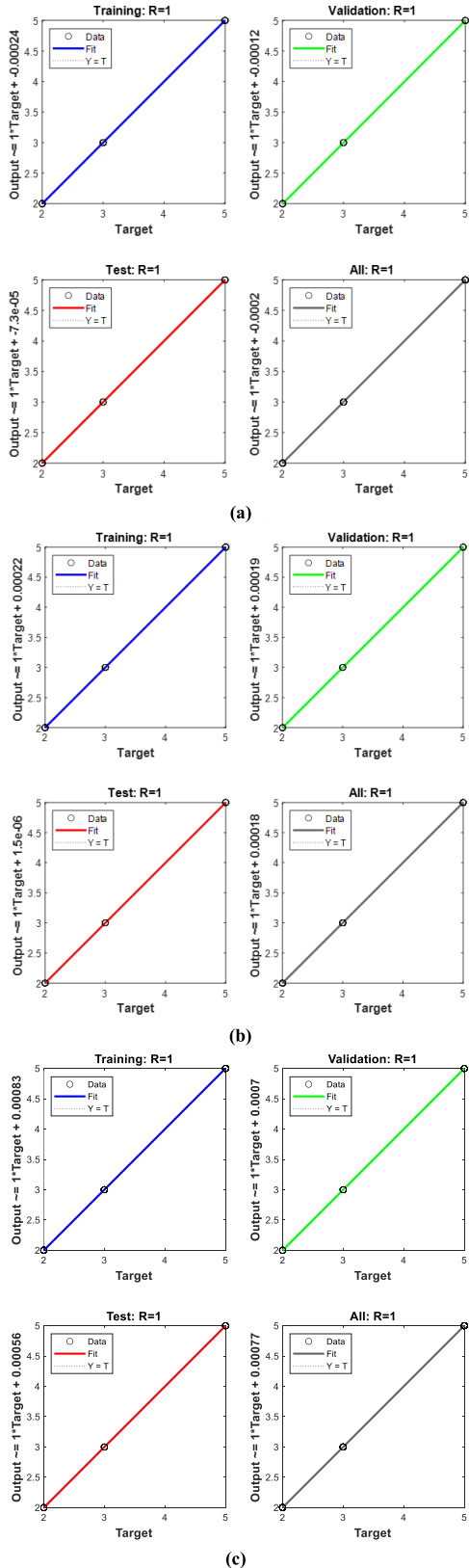


Fig. 10. Correlation coefficient diagram. (a) One layer, (b) two layers, and (c) three layers.

the predicted value and the actual value is stronger, and the fitting effect is better. When R is close to 0, there is no linear correlation between the predicted value and the actual

value, indicating that the model-fitting effect is poor. From the fitting curve and the corresponding correlation coefficient in the figure, it can be seen that the R -value in each data set under the three hidden layers is close to 1, indicating that there is a strong correlation between the predicted value and the actual value, which proves the validity and accuracy of the BP neural network on this problem. However, the R -values of each dataset are low under neural networks with one hidden layer and two hidden layers, and there may be an underfitting problem. Therefore, we believe that the neural network model with three hidden layers is the most suitable for predicting the magnetic induction data.

C. BP Neural Network Algorithm Prediction Experiment

To solve the calculation anomaly of the seventh layer in the nonlinear calculation process, further experiments were carried out, and a BP neural network was introduced for prediction. As a powerful nonlinear prediction method, the BP neural network can learn and approximate any function through training, has good nonlinear fitting ability and generalization ability, and can efficiently and accurately predict complex data. Experiments were designed in the three-axis Helmholtz coil. Two planes, XY and YZ, were selected for the path positioning experiment of the capsule robot. For the XY plane, the robot was placed in the coil along the z -axis, 50 mm away from the sensor. X , Y , square, and S-shape were selected in the XY plane for the positioning experiment. The positioning images are shown in Fig. 11(a), (b), (d), and (f), and the errors are shown in Fig. 11(f), (g), (i), and (j). Based on the experimental data, the positioning accuracy was calculated to be $1.019e-03$, $1.015e-03$, $3.282e-03$, and $3.532e-03$ mm. For the YZ plane, X and Y are fixed at 50 mm, and the robot is made to conduct positioning experiments along the z -axis. The positioning image is shown in Fig. 11(c), the error was shown in Fig. 11(h), and the positioning accuracy was $0.841e-03$ mm. In Fig. 11, the blue line represents the expected position of the capsule robot, and the red line represents the position predicted by the BP neural network. Compared with the calculation results of the previous nonlinear algorithm, the BP neural network can better predict the positioning path of the permanent magnet in the case of a sudden change in the seventh layer during nonlinear calculation, which improves the accuracy and reliability of the experiment.

As shown in Fig. 11(k) and (l), in the 3-D space experiment, one step is added sequentially along the z -axis direction, and the results are compared with the nonlinear calculation results. The results show that the BP neural network has a better predictive ability.

In Fig. 12, the corresponding error analysis is further carried out on the nonlinear calculation results and the prediction ability of the BP neural network. These experiments are for in-depth error analysis and research on the positioning ability of permanent magnets. By conducting experiments in three dimensions, we can gain a comprehensive understanding of the positioning capabilities of permanent magnets in different directions and the distribution of experimental errors. The experimental results show that the BP neural network has important application value in the permanent magnet

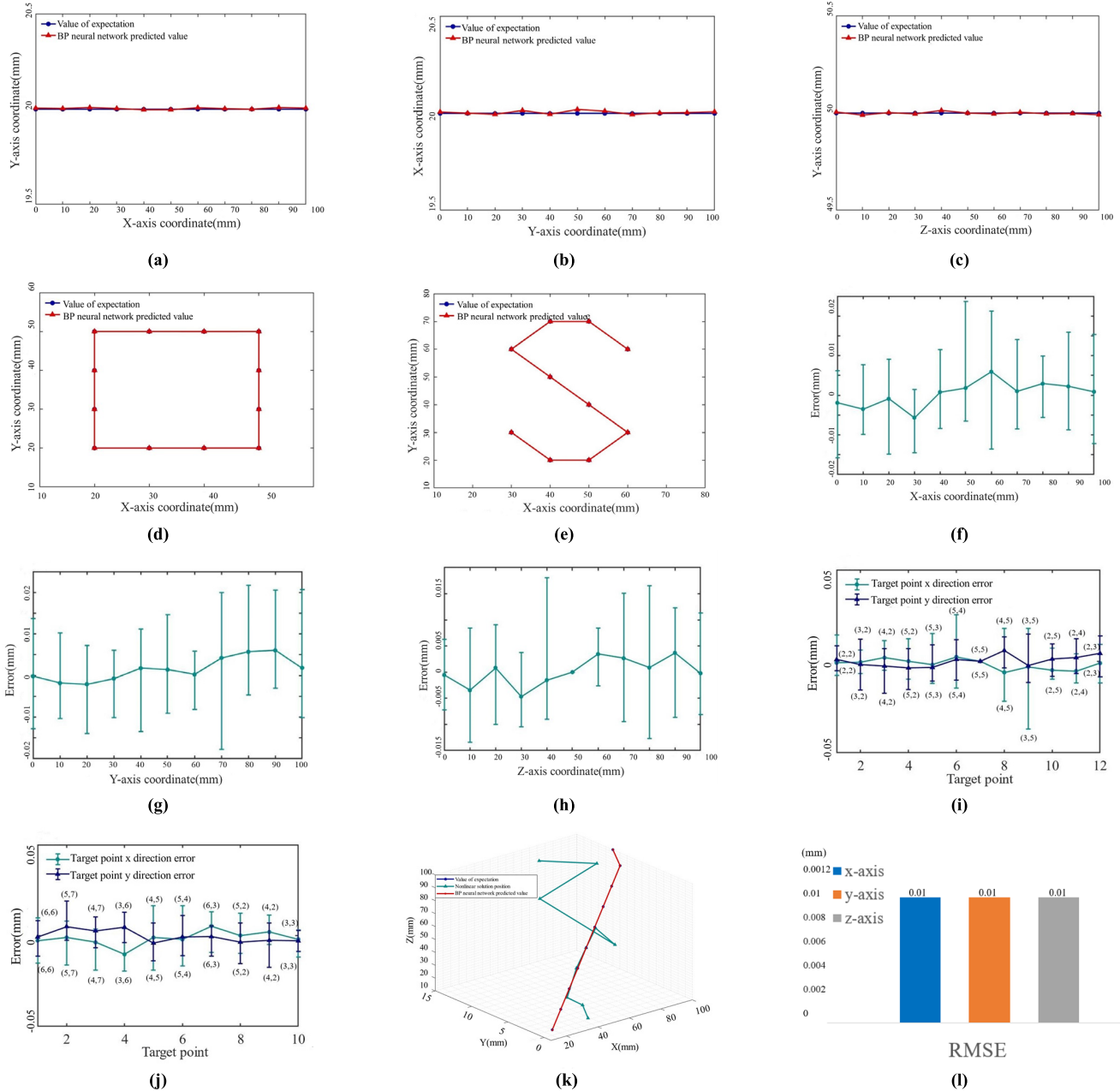


Fig. 11. BP neural network forecasting experiment. (a) x -axis direction. (b) y -axis direction. (c) z -axis direction. (d) Square path. (e) S-shaped path. (f) X -error. (g) Y -error. (h) Z -error. (i) Square-error. (j) S-error. (k) Space experiment. (l) Space experiment error.

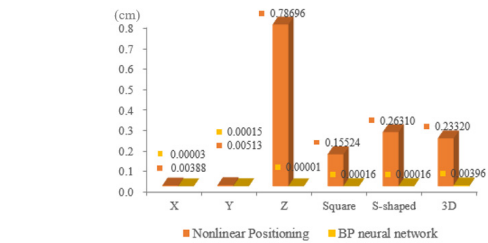


Fig. 12. Error analysis.

positioning, and can effectively improve the accuracy and reliability of the experiment. In future work, we will further explore the application potential of the BP neural network in the field of permanent magnet positioning, continuously

optimize its prediction accuracy and reliability, and provide better support and services for actual production and application.

V. CONCLUSION

This article addresses the localization and tracking problem of capsule endoscopy and proposes a prediction method based on BP neural network, which can use magnetic localization technology to locate the robot in the magnetic field. We designed a BP neural network model with three hidden layers and compared its prediction results with those of the nonlinear algorithm and the actual coordinate points. The experimental results show the localization rate of this model is 95.2%, which has higher localization accuracy and

optimization performance and can meet the real-time and localization accuracy requirements of capsule endoscopy. Our method provides an effective solution for capsule robots and other fields, with important application value and potential. In future work, we will further explore the application potential of the BP neural network in the permanent magnet localization field, and continuously optimize its prediction accuracy and reliability, to provide better support and service for practical production applications.

REFERENCES

- [1] P. R. Slawinski, N. Simaan, A. Z. Tadese, K. L. Obstein, and P. Valdastri, "Sensitivity ellipsoids for force control of magnetic robots with localization uncertainty," *IEEE Trans. Robot.*, vol. 35, no. 5, pp. 1123–1135, Oct. 2019.
- [2] C. Di Natali, M. Beccani, N. Simaan, and P. Valdastri, "Jacobian-based iterative method for magnetic localization in robotic capsule endoscopy," *IEEE Trans. Robot.*, vol. 32, no. 2, pp. 327–338, Apr. 2016.
- [3] C. Di Natali, M. Beccani, and P. Valdastri, "Real-time pose detection for magnetic medical devices," *IEEE Trans. Magn.*, vol. 49, no. 7, pp. 3524–3527, Jul. 2013.
- [4] D. Son, X. Dong, and M. Sitti, "A simultaneous calibration method for magnetic robot localization and actuation systems," *IEEE Trans. Robot.*, vol. 35, no. 2, pp. 343–352, Apr. 2019.
- [5] C. Hu et al., "A calibration method for the magnetic target tracking system," *J. Integr. Technol.*, vol. 3 no. 5, pp. 85–96, 2014.
- [6] C. Hu, M. Q.-H. Meng, M. Mandal, and X. Wang, "3-axis magnetic sensor array system for tracking magnet's position and orientation," in *Proc. 6th World Congr. Intell. Control Automat.*, vol. 2, Jun. 2006, pp. 5304–5308.
- [7] D. M. Pham and S. M. Aziz, "A real-time localization system for an endoscopic capsule," in *Proc. IEEE 9th Int. Conf. Intell. Sensors, Sensor Netw. Inf. Process. (ISSNIP)*, Apr. 2014, pp. 1–6.
- [8] G. Shao and Y.-X. Guo, "An optimal design for passive magnetic localization system based on SNR evaluation," *IEEE Trans. Instrum. Meas.*, vol. 69, no. 7, pp. 4324–4333, Jul. 2020.
- [9] S. Song, C. Hu, and M. Q.-H. Meng, "Multiple objects positioning and identification method based on magnetic localization system," *IEEE Trans. Magn.*, vol. 52, no. 10, pp. 1–4, Oct. 2016.
- [10] K. M. Popek, A. W. Mahoney, and J. J. Abbott, "Localization method for a magnetic capsule endoscope propelled by a rotating magnetic dipole field," in *Proc. IEEE Int. Conf. Robot. Automat.*, May 2013, pp. 5348–5353.
- [11] X. H. You, Z. Y. Zhang, Y. Zhang, and Y. Wang, "Six-dimensional hybrid positioning algorithm combining image positioning and magnetic sensor position for magnetically controlled capsule robot," *J. Zhejiang Univ. Eng. Sci.*, vol. 54, no. 11, pp. 2152–2162, 2020.
- [12] Z. Cai et al., "Characteristic analysis of a magnetically actuated capsule microrobot in medical applications," *IEEE Trans. Instrum. Meas.*, vol. 71, pp. 1–11, 2022.
- [13] Z. Song, W. Zhang, W. Zhang, and D. Paolo, "A novel biopsy capsule robot based on high-speed cutting tissue," *Cyborg Bionic Syst.*, vol. 2022, pp. 1–10, Jan. 2022.
- [14] Q. Fu et al., "A compensation method for magnetic localization on capsule robot in medical application," *IEEE Sensors J.*, vol. 21, no. 23, pp. 26690–26698, Dec. 2021.
- [15] Q. Fu, C. Fan, C. Wang, S. Zhang, and Z. Xi, "Improved magnetic positioning of medical capsule robot," *IEEE Sensors J.*, vol. 23, no. 15, pp. 17391–17398, Aug. 2023.
- [16] Q. Fu, X. Wang, J. Guo, S. Guo, and Z. Cai, "Magnetic localization technology of capsule robot based on magnetic sensor array," in *Proc. IEEE Int. Conf. Mechatronics Autom. (ICMA)*, Oct. 2020, pp. 267–272.
- [17] Q. Wang et al., "Retroreflection from a single layer of electromagnetic Helmholtz cavities based on magnetic symmetric dipole modes," *Opt. Exp.*, vol. 28, no. 21, pp. 30606–30615, 2020.
- [18] D. Z. Hua, "Research on key technologies of magnetorheological soft capsule robot," Ph.D. dissertation, School Mech. Elect. Eng., China Univ. Mining Technol., 2022.
- [19] G. K. Singh, A. Senthil Kumar, and R. P. Saini, "Selection of capacitance for self-excited six-phase induction generator for stand-alone renewable energy generation," *Energy*, vol. 35, no. 8, pp. 3273–3283, Aug. 2010.
- [20] X. Chen et al., "A novel artificial neuron-like gas sensor constructed from CuS quantum dots/Bi₂S₃ nanosheets," *Nano-Micro Lett.*, vol. 14, no. 8, pp. 1–15, Dec. 2022.
- [21] Y. Cui et al., "Investigation on the ignition delay prediction model of multi-component surrogates based on back propagation (BP) neural network," *Combustion Flame*, vol. 237, Mar. 2022, Art. no. 111852.
- [22] Q. Fu, J. Fu, J. Guo, S. Guo, and X. Li, "Gesture recognition based on BP neural network and data glove," in *Proc. IEEE Int. Conf. Mechatronics Autom. (ICMA)*, Oct. 2020, pp. 1918–1922.
- [23] Y. Li, F. Ding, and W. Tian, "Optimization of 3D printing parameters on deformation by BP neural network algorithm," *Metals*, vol. 12, no. 10, p. 1559, Sep. 2022.
- [24] X. Yi, "Selection of initial weights and thresholds based on the genetic algorithm with the optimized back-propagation neural network," in *Proc. 12th Int. Conf. Fuzzy Syst. Knowl. Discovery (FSKD)*, Aug. 2015, pp. 173–177.
- [25] H. Ye, L. Yang, and X. Liu, "Optimizing weight and threshold of BP neural network using SFLA: Applications to nonlinear function fitting," in *Proc. 4th Int. Conf. Emerg. Intell. Data Web Technol.*, Sep. 2013, pp. 211–214.
- [26] Y. Pan, Y. Wang, P. Zhou, Y. Yan, and D. Guo, "Activation functions selection for BP neural network model of ground surface roughness," *J. Intell. Manuf.*, vol. 31, no. 8, pp. 1825–1836, Dec. 2020.



Qiang Fu received the Ph.D. degree in intelligent mechanical systems engineering from Kagawa University, Takamatsu, Japan, in 2017.

He is currently an Associate Professor with the Tianjin University of Technology, Tianjin, China. His current research interests include biomedical robots and actuated micro-robotic systems for biomedical.



Dongdong Zhao is currently pursuing the master's degree with the School of Electrical Engineering and Automation, Tianjin University of Technology, Tianjin, China.

Her primary research interests include electromagnetic drive systems and target positioning of magnetic capsule robots.



Lei Shao is a Professor with the Tianjin University of Technology, Tianjin, China, and the Director of the Smart Energy IoT Application Research Institute, Tianjin, focusing on power electronics, such as autonomous robotics, the Internet of Things (IoT) monitoring technology, and digital workshop technology.



Songyuan Zhang (Member, IEEE) is currently an Associate Professor with the State Key Laboratory of Robotics and System, Harbin Institute of Technology, Harbin, China. His research interests include bio-inspired robotics, human–robot interaction, and medical robots.